Microwave-assisted hydrothermal synthesis of carbon doped with phosphorus for uranium(VI) adsorption

Lan Liu[1,2] · Xiaoyan Lin[1,2] · Mengsha Li[1] · Huanhuan Chu[1,2] · Hongyi Wang[1] · Yu Xie[1,2] · Zhichen Du[4] · Meijuan Liu[1] · Lili Liang[1,2] · Hongying Gong[1,2] · Jian Zhou[2] · Zhanguo Li[3] · Xuegang Luo[2]

Abstract
In this study, hydrothermal carbon doped with phosphorus using phytic acid (PA) and Sodium tripolyphosphate as functional monomers was successfully synthesized by the hydrothermal route combined with microwave-assisted hydrothermal carbon as matrix material. The uranium(VI) adsorption capacity by phytic acid functionalized microwave-assisted hydrothermal carbon (MHC-PA) was up to 382.2 mg/g at pH of 6.0 and the temperature of 298.15 K. The adsorption mechanism of uranium(VI) onto the MHC-PA was mainly the chelation of P=O, P–OH functional group and uranium(VI), which improves the selective adsorption performance of MHC-PA for uranium(VI).

Keywords Functionalization · Microwave-assisted hydrothermal carbon · Adsorption · Uranium · Adsorbent

Introduction

With the continuous development and utilization of nuclear energy, more and more uranium-containing radioactive wastewater is produced [1]. The discharge of uranium-containing wastewater into nature will cause immeasurable harm to the environment on which human beings depend. Today, this practice is even more undesirable when environmental protection issues are increasingly emphasized. Therefore, the treatment of uranium in uranium-containing wastewater has become an urgent problem [2].

✉ Xiaoyan Lin
lxy20100205@163.com

1 School of Materials Science and Engineering, Southwest University of Science and Technology, Mianyang 621010, Sichuan, China

2 Engineering Research Center of Biomass Materials, Ministry of Education, Mianyang 621010, Sichuan, China

3 State Key Laboratory of NBC Protection for Civilian, Beijing 102205, China

4 College of Materials Science and Engineering, Jilin University, Changchun, China

Compared with the main methods of treating uranium-containing wastewater, such as ion exchange [3], membrane [4], and adsorption [5–8], adsorption method is widely used in the treatment of uranium-containing wastewater in nuclear industry and other fields because of its simple preparation method, low cost and good treatment effect [9]. However, adsorption methods put forward higher requirements for the properties of adsorbents, such as: excellent acid–alkali resistance and thermal stability. For these reasons, carbon materials have become an ideal adsorbent [10].

The synthesis of carbon materials has a history of more than 3000 years since carbon black was synthesized. Among many synthesis methods, hydrothermal method has the advantages of simple operation conditions, low requirements for equipment, green reaction and no pollution to the environment [11]. However, there are some defects in the preparation of carbon materials by hydrothermal method, such as slightly higher preparation temperature, longer reaction time and high energy consumption [12]. Recently, with the development of microwave technology, it has been widely used in material chemical synthesis because of its selective heating, strong energy penetration, shorter reaction time, lower energy consumption, simple operation and uniform heating. The preparation of carbon materials by the microwave-assisted hydrothermal synthesis method has great advantages, which can greatly shorten the reaction time and improve the synthesis

efficiency. In recent years, the research on microwave-assisted hydrothermal synthesis of carbon materials has been favored by researchers [13, 14]. However, there were still some problems in microwave carbon materials, such as less functional groups and low selectivity for uranyl ion adsorption.

Phytic acid, also known as inositol hexaphosphate (PA, $C_6H_{18}O_{24}P_6$) was a non-toxicity, odorless, harmless organic compound, widely found in seeds and pollens of legumes, maize, brown rice, sesame, wheat bran and other plants. The six phosphate groups in PA structure endowed it with strong chelating metal cations ability [15]. The capacity of phytic acid chelating with metal ions via a strong coordination bond make phytic acid a potential chelating agent for uranium. In recent years, the study of phytic acid as modifier has attracted widespread attention. Hao et al. studied that phytic acid impregnated polyaniline (PA-PANI) was synthesized by in situ polymerization and supramolecular self-assembly with phytic acid as modifier. It was an effective adsorbent for uranium capture from aqueous solution. A series of adsorption results showed that the U(VI) adsorption capacity of PA-PANI-3 increased by 86.6 mg/g, greatly exceeding that of polyaniline (PAN, 8.8 mg/g) [16]. Wang et al. used phytic acid as a functional reagent to synthesize a new two-dimensional graphene oxide material, and had good adsorption capacity for Cu(II) ions. The experimental results showed that the material achieved equilibrium adsorption within 20 min and the maximum adsorption capacity was 316.6 mg/g [17]. Liu et al. synthesised graphene oxide/phytic acid sponge composite material, and the maximum adsorption capacity of U(VI) was 124.3 mg/g at pH 5.5. We can concluded that the introduction of phytic acid moieties exhibited favorable adsorption performance for U(VI) [18]. Moreover, sodium tripolyphosphate is a chain like condensed phosphate, which is a kind of phosphate, has strong chelating ability with metal ions Ca^{2+}, Mg^{2+}, Cu^{2+}, Fe^{2+} and other metal ions, mainly used in the treatment of industrial water and important components of detergents. With the wide application of sodium tripolyphosphate, its physical and chemical properties have been widely studied [19].

Hence, in this study, the microwave-assisted hydrothermal carbon microspheres (MHC-COOH), which was synthesized earlier by our research group, were used as the carbon matrix, and then modified by phytic acid (PA) and sodium tripolyphosphate (STPP) respectively. Finally, the phosphorus-containing carbon materials denoted as MHC-PA and MHC-STPP, were obtained by traditional hydrothermal method. Different techniques, such as SEM, FTIR, XPS, TGA and BET, have been used to characterize the surface morphology, functional groups and skeleton properties of MHC-PA and MHC-STPP. Then, the adsorption performance of MHC-PA was studied in detail.

Experimental

Materials

Glucose ($C_6H_{12}O_6$), hydrated $AlCl_3$, phytic acid (PA, $C_6H_{18}O_{24}P_6$, 50%), sodium tripolyphosphate ($Na_5P_3O_{10}$), uranium nitrate hexahydrate ($UO_2(NO_3)_2 \cdot 6H_2O$) were provided by Chengdu Kelong Co., Ltd.,China. All used reagents were of analytical pure and without further purification.

Preparation of samples

Synthesis of microwave-assisted hydrothermal carbon (MHC-COOH)

MHC-COOH was prepared according to method as Ref. [20]. 1.58 g of glucose and 0.23 g of $AlCl_3$ were dissolved in 30 ml deionized water which formed a mixed solution with strong stirring. Then the mixed solution was poured in microwave reaction vessel being made of Teflon (XH-800C, Beijing Xianghu, China) under a magnetron frequency of 2.45 GHz, power of 700 W and pulse controlled power fractions of 10 W and heated for 8 h at 130 °C. Subsequently, after the reaction vessel being cooled to room temperature, the product was washed alternately with absolute ethanol and deionized water until the filtrate was nearly neutral, and then being vacuum dried overnight at 60 °C. The collected products were further calcined in muffle furnace for 5 h at 300 °C. The aim of calcination is to increase the amount of functional groups (mainly carboxylic groups) on the surface of carbon spheres to provide a better matrix for subsequent functional modification, and then the carboxylic carbon spheres was labeled as MHC-COOH.

Synthesis of microwave-assisted hydrothermal carbon doped with phosphorus

0.1 g MHC-COOH was added in beaker containing 68.9 mL deionized water, after that, 1 mL phytic acid was added to the above beaker, magnetic stirred and sonicated for 20 min to form a uniform solution. Then the mixture solution was transferred to 100 mL Teflon-lined stainless steel autoclave and heated for 12 h at 95 °C. The obtained products was soaked in deionized water for 24 h in order to remove the residuals and then centrifuged, filtered. Finally, the product named as MHC-PA was obtained throughout vacuum dried for 24 h.

0.1 g MHC-COOH was added in beaker containing 68.5 mL deionized water, after that, 1.4 g sodium

tripolyphosphate was added to the above beaker, magnetic stirred and sonicated for 20 min to form a uniform solution. The subsequent method is the same as the synthesis method of the above material (MHC-PA). The prepared material is called MHC-STPP.

Uranium adsorption experiments

To study the adsorption performances of MHC-PA for uranium(VI), the batch sorption experiments were carried out in 140 r/min constant temperature vibration incubator. Typically, a certain amount of adsorbent and 20 mL uranium(VI) solution with different concentrations were put into erlenmeyer flask. The effects including pH, dosage, contact time, temperature and initial concentration of uranium etc. on the adsorption amount of uranium(VI) had been performed. The initial pH varied from 1 to 7 regulated by negligible amount of 1 mol/L HCl and 1 mol/L NaOH solutions. The dosage of adsorbents varied from 0.001 to 0.007 g and contact time changed from 30 to 1440 min. The temperature ranged from 288.15 to 328.15 K and initial concentration of uranium(VI) at the range of 20–140 mg/L.

The remaining uranium(VI) concentrations were tested using the methods of arsenazo III by a UV–visible spectrophotometer at 650 nm [11]. The amount of uranium adsorbed per unit mass of the sorbent q_e (mg/g) at equilibrium and removal efficiency RE (%) were calculated by the following equation [21]:

$$q_e = \frac{(C_0 - C_e)V}{m} \tag{1}$$

$$RE = \frac{C_0 - C_e}{C_0} \times 100\% \tag{2}$$

where C_0 (mg/L) and C_e (mg/L) are the concentration of uranium(VI) in initial and equilibrium of the solution respectively, V (L) is the volume of uranium(VI) solution used for adsorption, m (g) denotes the mass of dried adsorbents added in uranium(VI) solutions. All of the experiments were carried out in three batches.

Characterization of the adsorbent

The surface morphology and element composition of samples was observed by a field-emission scanning electron microscopy (SEM, Zeiss Ultra 55; Zesis Corporation, Germany) coupled with Energy Dispersive X-Ray Spectroscopy (EDX, Ultra 55, Carl Zeiss, Germany). The types of functional groups was measured with fourier transform infrared spectroscopy (FTIR, Nicolet-6700; Perkin Elmer Instruments Corporation, USA). The element composition and distribution were analysed by X-ray photoelectron spectroscopy (XPS, Escalab 250, Thermo Fisher Corporation, USA). The thermal decomposition performance were carried out by a thermogravimetric analyzer (TGA, TGAQ500, TA Instruments, USA) at a heating rate of 20 °C/min from 35 to 800 °C under nitrogen atmosphere.

Results and discussion

SEM analysis

The surface morphology of MHC-COOH, MHC-PA and MHC-STPP was examined by scanning electron microscopy shown in Fig. 1. From Fig. 1a, it can be clearly observed the good dispersity of microspheres without serious agglomeration between MHC-COOH microspheres. However, minor adhesion of MHC-PA could be observed in Fig. 1b, resulting from the PA reaction with MHC-COOH microspheres, in which PA acts as a bridge between carbon microspheres. Compared the enlarged view in Fig. 1a with that in Fig. 1b of carbon material before and after phytic acid modification, it can be found that there is no obvious change in the shape and structurethe before and after modification. However, the surface of carbon microspheres before modification is smooth, while the surface of carbon microspheres after modification is slightly rough. This reveals that the modification of phytic acid has no obvious effect on the spherical structure of carbon materials manifesting its good chemical stability in the process of phytic acid modification. Phytic acid can change the surface structure and increase the roughness of carbon
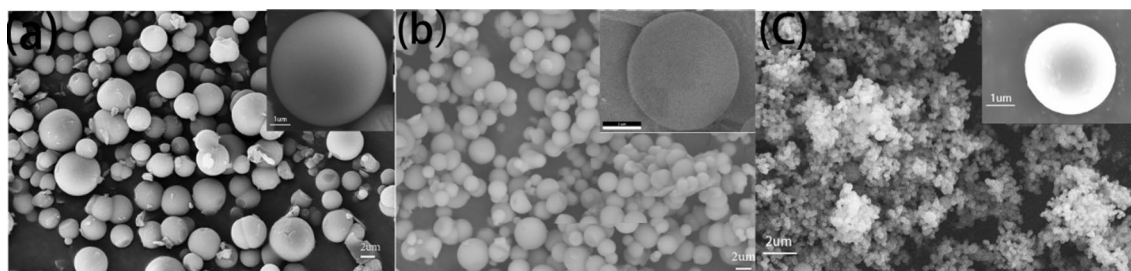

Fig. 1 SEM images of **a** MHC-COOH, **b** MHC-PA, **c** MHC-STPP

microspheres, which is beneficial to the improvement of the adsorption properties.

It can be seen from Fig. 1c that the modification of the MHC-COOH microsphere by sodium tripolyphosphate greatly reduces the particle size of carbon microsphere to nanometer level. This may be the solubilization of sodium tripolyphosphate can make liquid and solid particles better soluble in aqueous solution.

FT-IR analysis

In order to clearly understand the types of bonds between phytic acid, sodium tripolyphosphate and carbon microspheres respectively, we further made FTIR analysis of carbon microspheres. The FT-IR spectra of MHC-COOH, MHC-PA, MHC-STPP were shown in Fig. 2. In the FT-IR spectra of MHC-COOH, the broad band at ~ 3433 cm^{-1} can be assigned to the stretching vibration of hydroxyl groups [22]. The bands at 1715 cm^{-1} was assigned to the C=O stretching vibrations of the carboxyl groups, and the band at ~ 1617 cm^{-1} assigned to the stretching mode of –C=C– groups of aromatic ring [23]. After modification of the MHC-COOH by phytic acid, the absorption peak intensity at 1715 cm^{-1} decreased, the stretching vibration peak of aromatic ring –C=C– group moved from 1617 to 1628 cm^{-1}, and the corresponding absorption peak position of –OH moved from 3433 to 3434 cm^{-1}, indicating that the deformation of aromatic ring which could be caused by the interaction of oxygen-containing group C=O and PA through hydrogen bond [24]. The FT-IR spectrum of MHC-PA clearly exhibits two peaks at 1256 cm^{-1}, 1062 cm^{-1}, which can be assigned to P=O and P–O–C groups [25].
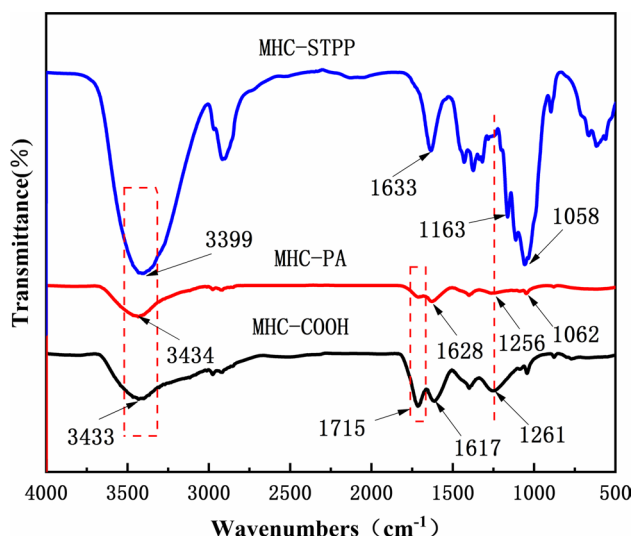
These results all proved that phytic acid was successfully grafted onto MHC-COOH microspheres.

Comparing the FT-IR spectra of MHC-STPP with MHC-COOH, we can see that the absorption peak at 1715 cm^{-1} disappeared after the modification of the MHC-COOH by sodium tripolyphosphate, the stretching vibration peak of –C=C– group moved from 1617 to 1633 cm^{-1}, and the corresponding absorption peak of –OH moved from 3433 to 3399 cm^{-1}, which indicated that the C=O group on the surface of MHC-COOH reacted with sodium tripolyphosphate. The absorption peak at 897 cm^{-1} in the FT-IR spectrum of MHC-STPP belongs to the antisymmetric stretching vibration of P–O–P group, and the absorption peak of 1170–1010 cm^{-1} (1058 cm^{-1}, 1113 cm^{-1}, 1163 cm^{-1}) belongs to the symmetric and antisymmetric stretching vibration of PO_2 and PO_3 group [26]. The results showed that sodium tripolyphosphate successfully modified microwave-assisted hydrothermal carbon microspheres.

EDX analysis

In order to comprehensively analyze the distribution of phytic acid and sodium tripolyphosphate on the surface of carbon microspheres, the energy spectrum analysis of the functionalized carbon materials is carried out, and the results were shown in Fig. 3. Figure 3 are the element distribution diagram of EDX of the functionalized carbon materials. From Fig. 3b, it can be seen that the element composition of MHC-PA is C, O and P. the appearance of P indicates that phytic acid successfully interacts with the surface of carbon microspheres. From the element distribution diagram, it can be seen that P distribution is relatively uniform, which indicates that phytic acid uniformly interacts with carbon microspheres. From Fig. 3a, it can be seen that the element composition of MHC-STPP is C, O, P, Na. The content of P and Na elements is less, indicating that the binding amount of sodium tripolyphosphate and hydrothermal carbon is less.

The effect of modification on the adsorption capacity of the carbon microspheres for uranium

The above characterization shows that both phytic acid and sodium tripolyphosphate have been successfully bonded to microwave-assisted hydrothermal carbon. In order to further explore the effect of functional modification by phytic acid and sodium tripolyphosphate on the adsorption performances of the carbon microspheres for uranium(VI), the carbon materials of MHC-COOH, MHC-PA and MHC-STPP with adsorbent dosage of 0.005 g respectivly, were put into the uranium solutions with the initial uranium(VI) concentration of 20 mg/L and the initial pH of 6 at 298.15 K. The sorption experiments were carried out in 140 rpm being

Fig. 2 FTIR spectra of MHC-COOH, MHC-PA and MHC-STPP
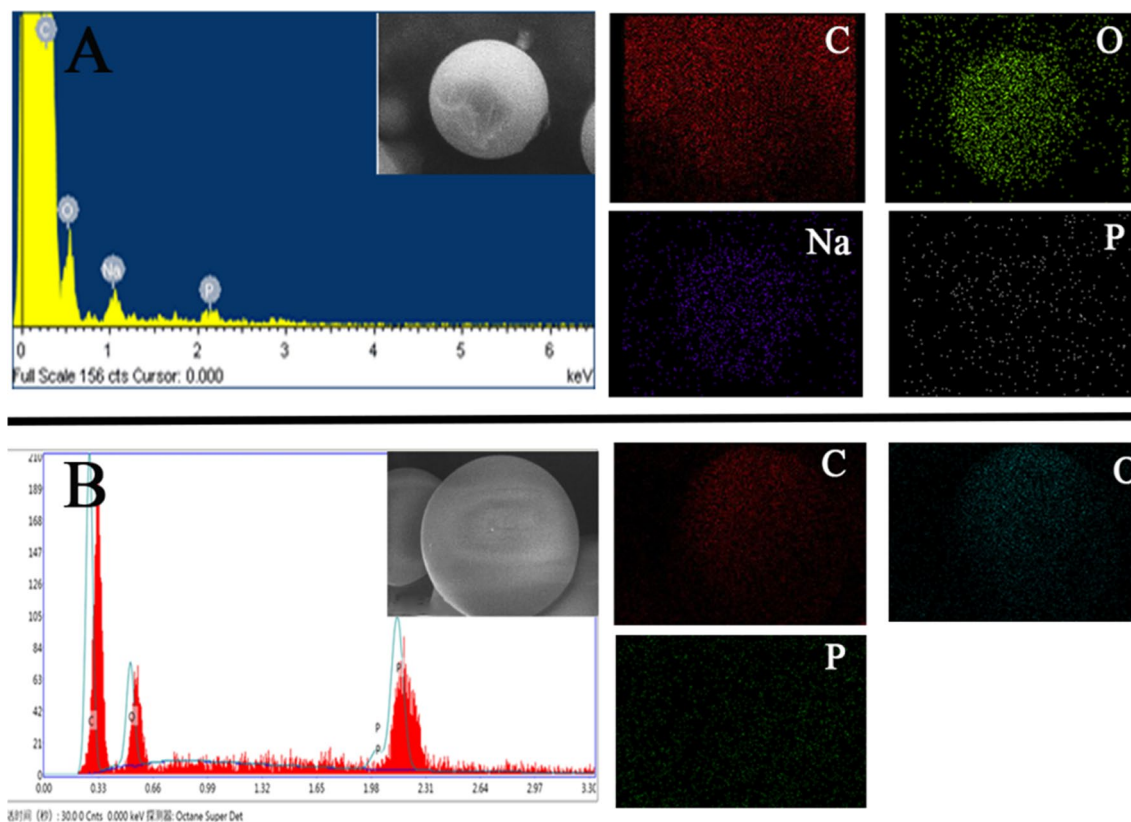
Fig. 3 EDX images of MHC-STPP and MHC-PA

oscillated for 1440 min at constant temperature vibration incubator.

The results of sorption experiments showed that the uranium adsorption capacity of MHC-COOH, before modification by phytic acid and sodium tripolyphosphate, was 52.76 mg/g. However, the adsorption capacity of MHC-PA and MHC-STPP, after modification by phytic acid and sodium tripolyphosphate, for uranium is higher than that of MHC-COOH. It can also be seen that the adsorption capacity of MHC-PA is 382 mg/g, higher than that of MHC-STPP (266 mg/g), which disclosed that the functional groups in the surface of microwave-assisted hydrothermal carbon were significantly increased by the functional modification of phytic acid and sodium tripolyphosphate resulting in the adsorption performance of carbon material for uranium is significantly improved. Compared with phytic acid modification, the adsorption capacity improvement of MHC-STPP is slightly lower. Therefore, the follow-up study will further focus on analysis of the surface structure, thermal stability and adsorption characteristics of MHC-PA.

XPS analysis

X-ray photoelectron spectroscopy (XPS) analysis was an effective technique to identify and quantitatively measure the surface compositions and binding condition of materials. The XPS spectrum of MHC-PA, MHC-COOH with the binding energy of 0–1200 eV range were presented in Fig. 4. For the MHC-COOH, the peaks of C1s and O1s can be obviously observed from the Fig. 4a, b. Four major peaks of the C1s located at 284.76 eV, 286.41 eV, 288.77 eV and 291.26 eV were assigned to the C=C/C–C, C–O, C=O and O-C=O peaks, respectively and the O1s peaks at 531.61 eV, 532.56 eV, 533.05 eV and 533.79 eV were related to the O=C, O–C=O, C–O–C and –OH groups [24, 27], respectively. After the PA modified the MHC-COOH, there were obvious differences in several peaks of the XPS spectrum with that of MHC-COOH. A new small band emerged at 134 eV was attributed to the P2p peaks as depicted in Fig. 4e, indicting that PA was successfully connected with the MHC-COOH [28]. These results are consistent with the FTIR Fig. 2. In addition, we can see from Fig. 4c, d that the C1s peaks of C=C/C–C (284.74), C–O (286.37), C=O (288.82) and O–C=O (291.61) and the O=C (531.73), O–C=O (532.64), C–O–C (533.17) and –OH (533.77) groups of O1s could still appeared but the peak intensities decreased. Moreover, the new species assigned to the typical P–O peak was also
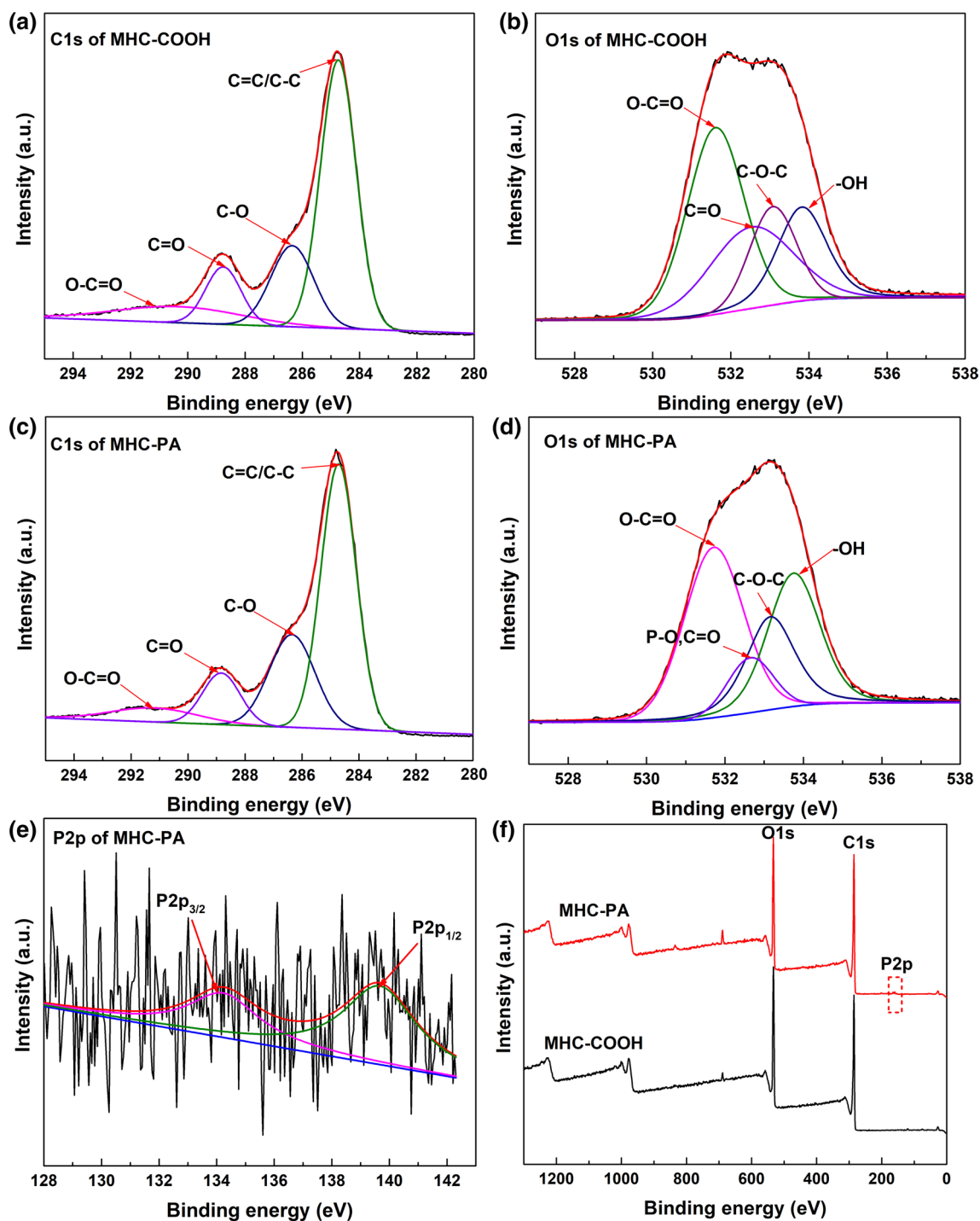
Fig. 4 XPS high resolution spectra of **a** C1s and **b** O1s for MHC-COOH; **c** C1s, **d** O1s and **e** P2p for MHC-PA; **f** XPS survey spectrum of MHC-COOH and MHC-PA

emerged at 532.64 eV and the high resolution spectra for P2p peaks was recorded and analyzed in detail seen in Fig. 4d [28]. In brief, all of these results above suggested that PA had modified MHC-COOH successfully.

BET analysis

Figure 5 showed the nitrogen adsorption desorption isotherm model of MHC-COOH and MHC-PA. The specific surface area, total N_2 desorption volume and average desorption pore diameter of the two materials were listed in
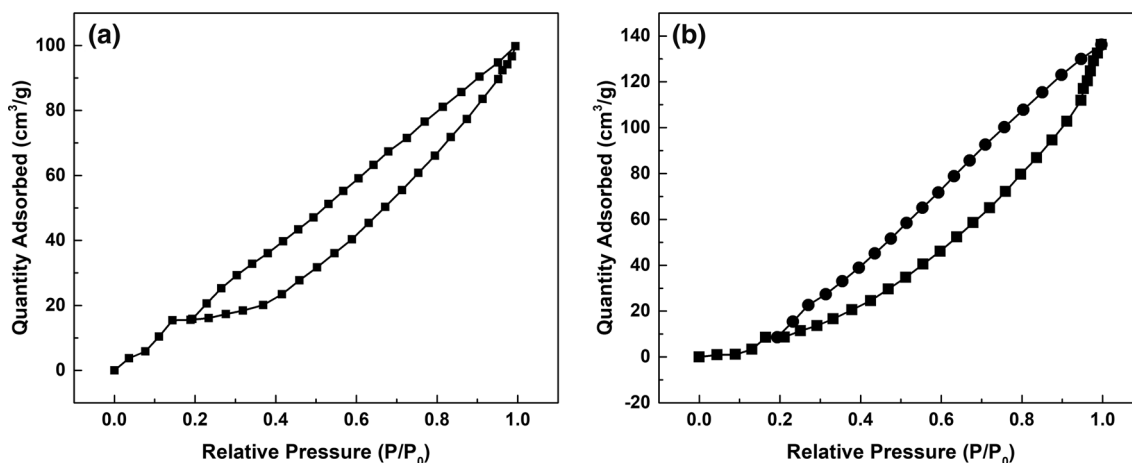
Fig. 5 Nitrogen adsorption–desorption isotherms of **a** MHC-COOH and **b** MHC-PA
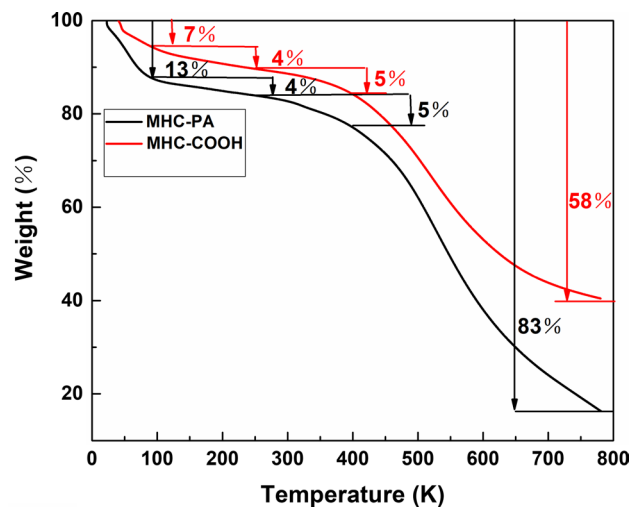
Table 1 Specific surface, pore volume and average pore size of MHC-COOH and MHC-PA

Sample	Specific surface (m²/g)	Porevolume (cm³/g)	Average pore size(nm)
MHC-COOH	61.682	0.216	4.296
MHC-PA	67.395	0.211	4.412

Fig. 6 TGA curves of the MHC-COOH, MHC-PA samples at a heating rate of 10 °C/min under a nitrogen flow

Table 1. It can be seen from Table 1 that the specific surface area of the MHC-PA increased slightly and the pore size and volume did not change significantly, indicating that the modification of phytic acid did not change the porous structure and specific surface area of the MHC-COOH microspheres, only with the PA being grafted to the surface of MHC-COOH. This result is consistent with that of the previous SEM analysis.

TGA analysis

The thermal stability of the carbon materials plays an important role in the application of waste water treatment. Figure 6 showed the TGA curve of MHC-COOH and MHC-PA under the nitrogen atmosphere at a temperature range of 35–800 °C. According to Fig. 6, the weight loss curve of MHC-COOH and MHC-PA carbon material is almost similar. For MHC-COOH, the weight loss is 7% in the range of 35–100 °C, which is mainly caused by the loss of residual water in carbon microspheres. In the range of 100–400 °C, the weight loss is 9%, which is mainly caused by the decomposition of oxygen-containing groups. When the temperature is over 400 °C, the weight loss increased significantly, which is mainly due to the partial decomposition of carbon microspheres. For MHC-PA carbon microsphere materials, the first stage of weight loss occurs between

35 and 100 °C, 13% of weight loss is due to the loss of residual water, and the second stage occurs between 100 and 250 °C, 4% of weight loss is mainly due to the decomposition of non reactive phytic acid molecules (~ 193 °C) and oxygen-containing groups of carbon materials. When the temperature is between 250 and 400 °C, the mass loss of 5% comes from the decomposition of OH group in PA and oxygen group in carbon material, and obvious mass loss occurs after 400 °C, which is related to the decomposition of phytic acid group and carbon microspheres [29]. When the temperature continued rising to 800 °C, there was a significant difference in weight loss of both MHC-COOH and MHC-PA. The mass loss of MHC-COOH is 58%, but that of MHC-PA is 83%. It can be concluded that the thermal stability of MHC-PA is slightly weaker than that of MHC-COOH
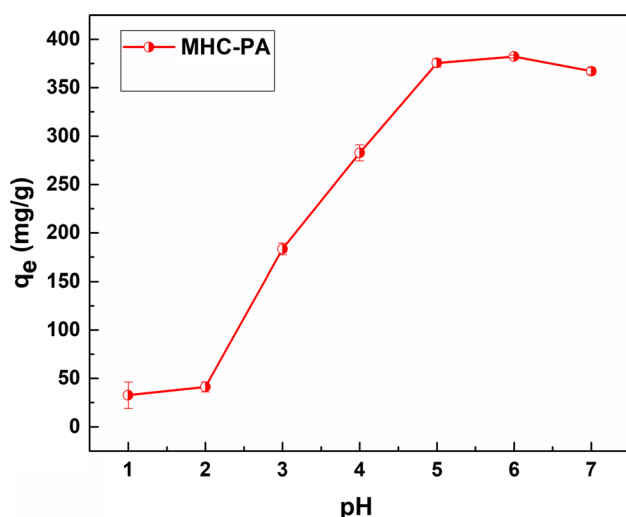
at high temperature, this may be due to that there is a strong hydrogen bonding between phytic acid and surface groups of microwave-assisted hydrothermal carbon during the modification process which was dissociated with the temperature greater than 4. However in the range of 100–400 °C, the weight loss of MHC-PA and MHC-COOH are both 9%, which indicated that MHC-PA has the same good thermal stability as MHC-COOH at low temperature.

Adsorption characteristics of the MHC-PA microspheres for uranium(VI)

Effect of pH

The values of pH impacts the uranium species and the functional group activity of adsorbents in the adsorption process [30]. In order to evaluate the effect of pH on the adsorption amount of uranium(VI), a certain amount of MHC-COOH and MHC-PA were put into the uranium solutions with the initial uranium(VI) concentration of 20 mg/L, and the initial pH ranging from 1 to 7 at 298.15 K. The results were shown in Fig. 7. The adsorption amount of MHC-PA microspheres for uranium(VI) strongly depended on the pH of solution, and reached to the maximum value of 382.20 mg/g at pH 6, which was much more higher than that of the MHC-COOH (52.76 mg/g). This showed that the MHC-PA had excellent adsorption capacity, which may be due to the addition of a large number of –OH and P=O active functional groups on the surface of the MHC-PA.

When the pH value was below 6, the adsorption capacity increased with the increase of pH value. The best adsorption performance o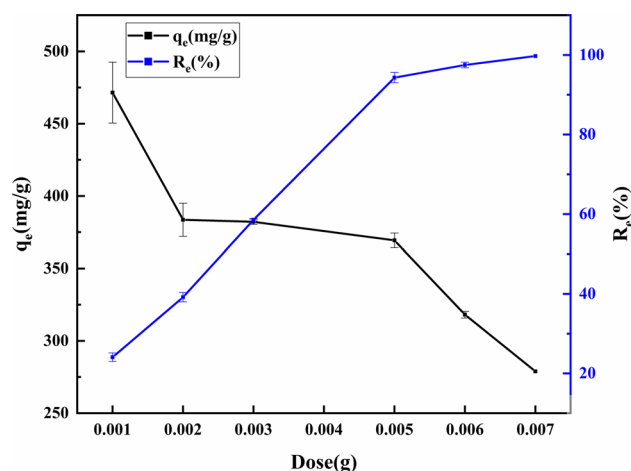f MHC-PA was presented at pH 6. It could be supposed that the active sites on the surface of MHC-PA were occupied by hydrogen ions at low pH, and electrostatic exclusion between hydrogen ions and uranyl ions will increase. Moreover, due to the protonation of carboxyl and hydroxyl groups on the surface of the MHC-PA material, the contact opportunities between oxygen-containing groups on MHC-PA carbon materials and uranium ions were reduced, which leaded to a low adsorption amount [31]. With the increase of pH, the UO_2OH^+, $(UO_2)_3OH^{5+}$ and $(UO_2)_2(OH_2)^{2+}$ hydrate in the aqueous solution were dominant which decrease the electrostatic exclusion combing with the deprotonation of the MHC-PA which lead to the increase of adsoption capacity. Then when the pH was beyond 6, the adsorption amount of MHC-PA started to decrease gradually. The main reason was negatively charged of $(UO_2)_3(OH)_7^-$ (a kind of uranium hydrate) started occur when the pH was beyond 6 [12, 32] which lead to the electrostatic repulsion of PA with uranium hydrate. So the adsorption amount would be declined. As a result, the best adsorption amount of MHC-PA for uranium(VI) was obtained at pH 6.

Effect of adsorbent dosage

It is important to study the effect of adsorbent dosage on adsorption capacity and the removal efficiency of MHC-PA microspheres for uranium(VI). The corresponding results were shown in the Fig. 8. We can see that the removal efficiency increased gradually with increasing of adsorbent dosage, which may be due to the increase of active sites and contact area with uranium(VI) [33]. On the contrary, the adsorption capacity decreased, this may be due to the fact that with the increase of the adsorbent dosage, the amount of uranium(VI) adsorbed by a unit mass of material will
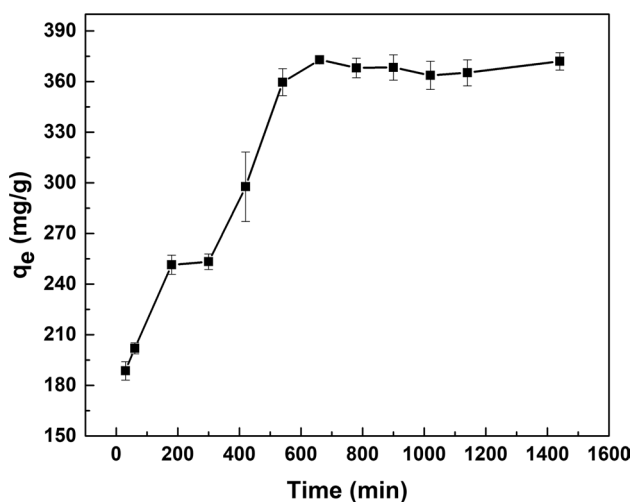

Fig. 7 Effect of the pH on the adsorption of uranium(VI) onto the MHC-PA (MHC-PA: C_0: 20 mg/L, t: 24 h, V: 100 mL, T: 298.15 K and m: 0.005 g)

Fig. 8 Effect of the adsorbent dose on the adsorption of uranium(VI) onto the MHC-PA (C_0: 20 mg/L, t: 24 h, V: 100 mL, T: 298.15 K and pH: 6)

decrease and the phenomenon of unsaturation appeared in a certain amount of uranium(VI) solution [34]. When the adsorption dosage is 0.005 g, the removal efficiency reaches 95%. With further increasing the adsorption dosage, the removal efficiency would approach to 100% and tend to balance gradually. Considering the better removal efficiency and adsorption capacity, 0.005 g was selected as the adsorbent dosage of the following series of adsorption experiments.

Effect of contact time and adsorption kinetics

Contact time was a significant factor providing effective information for reaction kinetics and adsorption mechanism. The effect of contact time varying from 0 to 24 h

Fig. 9 Effect of contact time on the adsorption of uranium(VI) onto the MHC-PA (C_0: 20 mg/L, pH: 6, V: 100 mL, T: 298.15 K and m: 0.005 g)

on the adsorption amount of MHC-PA for uranium(VI) was shown in Fig. 9. It was observed that the amount of uranium(VI) adsorbed on MHC-PA increased sharply during the first 540 min and then gradually reached to equilibrium at 660 min. The adsorption process of U(VI) onto MHC-PA was ultra-fast during the early stage which can be owing to the larger concentration gradient and a large number of active sites available for adsorption. While with the decrease of adsorption active sites, the adsorption rate reduced and reached gradually equilibrium at 660 min.

The mechanism of controlling the adsorption process was explained by pseudo-first-order and pseudo-second-orderkinetic models, and the equations were given as follows [35, 36]:

$$\ln\left(q_e - q_t\right) = \ln q_e - k_1 t \tag{3}$$

$$\frac{t}{q_t} = \frac{t}{q_e} + \frac{1}{k_2 q_e^2} \tag{4}$$

where q_e (mg/g) and q_t (mg/g) are the uranium amount adsorbed on the sorbent at equilibrium and given time t (min) respectively. k_1 (min^{-1}) and k_2 (g/(mg min)) are rate constants of pseudo-first-order and pseudo-second-order kinetic model respectively, which could be calculated by slope and intercept of the fitting curves.

The results of two models were showed in Fig. 10 and Table 2, from which we can clearly see the difference between the kinetic parameters of the two models. The square of correlation coefficients (R^2) vaule of pseudo-second-order (0.99) was better than that of pseudo-first-order model (0.88), which indicated the fitting degree of pseudo-second-order model was more higher than that of pseudo-first-order. Moreover, the pseudo-second-order model q_e (395.26 mg/g) was closer to the experimental
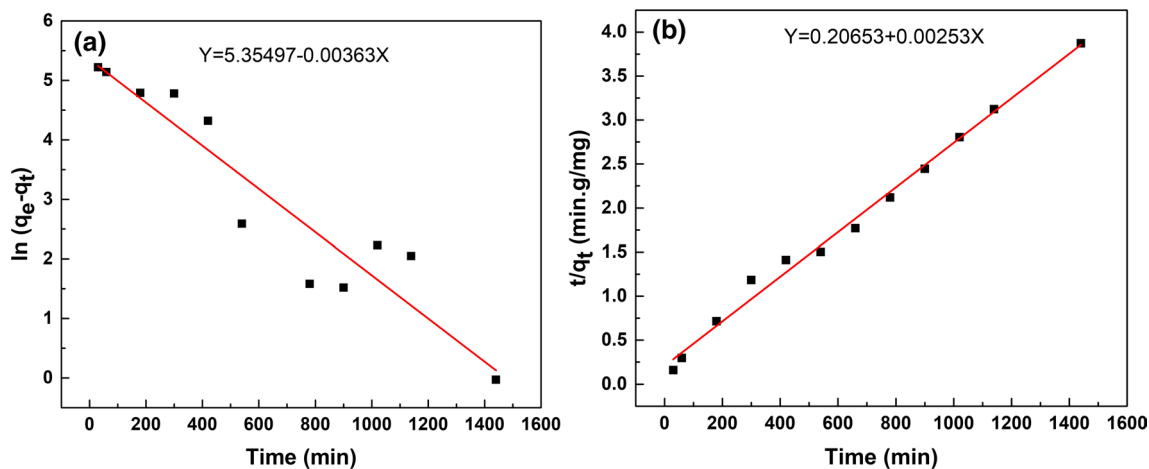
Fig. 10 **a** pseudo-first-order kinetics and **b** pseudo-second-order kinetics plots for uranium(VI) adsorption on MHC-PA, respectively

Table 2 Kinetic parameters for the uranium(VI) adsorption onto MHC-PA microspheres

Model	Pseudo-first-order model			Pseudo-second-order model		
Parameter	q_e (mg/g)	k_1 (g/mg min)	R^2	q_e (mg/g)	k_2 (g/mg min)	R^2
Value	211.66	0.00363	0.88	395.26	3.09×10^{-5}	0.99
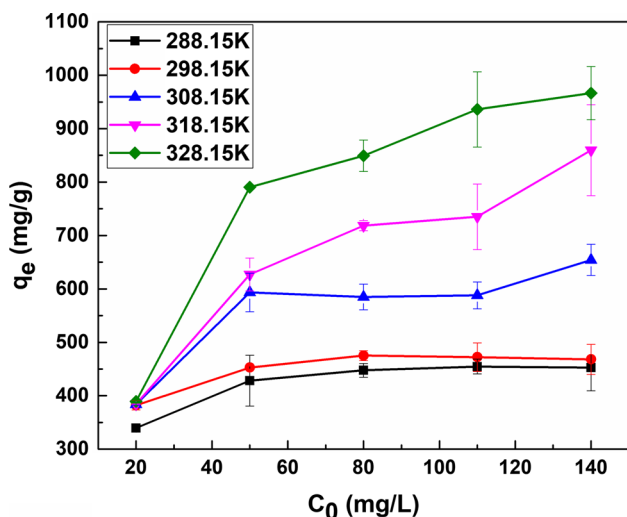
Fig. 11 Effect of initial uranium(VI) concentration on the adsorption of uranium(VI) onto the MHC-PA (*t*: 24 h, pH: 6, *V*: 100 mL and *m*: 0.005 g)

values 382.20 mg/g than pseudo-first-order model q_e (211.66 mg/g). Therefore, the adsorption process of U(VI) can be described by the pseudo-second-order model, which indicated that the chemisorption was the rate-determining step [37]. And the chemisorption reaction happening between the adsorbate and asorbent was probably the coordination of uranium with –OH or P=O.

Effect of initial concentrations on adsorption and isotherm models

The effect of initial uranium(VI) concentrations on adsorption of MHC-PA were determined with varying the initial uranium(VI) concentrations from 20 to 140 mg/L and revealed in Fig. 11. When the initial concentration is lower than 50 mg/L, in the temperature range of 288.15–328.15 K, the adsorption capacity of MHC-PA for uranium(VI) increases rapidly with the increase of the initial uranium(VI) concentration, which may be due to the action of concentration gradient to increase the adsorption rate of uranium(VI). When the initial concentration is higher than 50 mg/L and the temperature is 288.15–308.15 K, the adsorption capacity of MHC-PA to uranium(VI) increases slowly with the increase of initial uranium(VI) concentration. Inconsistently, when the temperature is higher than 308.15 K and the initial concentration is higher than 50 mg/L, the adsorption

capacity continues to increase greatly with the increase of initial concentration. In addition, in the low initial concentration, the adsorption capacity increases slowly with the increase of temperature, while in the high initial concentration, the adsorption capacity increases significantly with the increase of temperature. The probable reason was that with the increase of temperature, the uranium ions movements was enhanced leading to its favorable for more uranium ions coordination with MHC-PA. Finally it showed that adsorption equilibrium would appear at higher initial concentration at higher temperature.

In order to further understand the form and mechanism of uranium(VI) adsorption onto the adsorbent surface, the Langmuir, Freundlich, the Temkin and the Dubinin–Radushkevich (D–R) models were fitted for sorption isotherms. The Langmuir isothermal model was based on the assumptions of adsorption homogeneity, in which there was no reaction between the adsorbent molecules and the energy of adsorption sites was equivalent. It was a monolayer adsorption behavior and the linear and non-linear Langmuir isotherm equation can be expressed as equation [38]:

$$\frac{C_e}{q_e} = \frac{1}{K_L q_m} + \frac{C_e}{q_m} \text{(linear)} \tag{5}$$

$$q_e = \frac{K_L q_m C_e}{1 + K_L C_e} \text{(non - linear)} \tag{6}$$

The Freundlich isotherm model assumed that the adsorption was multilayer sorption with a heterogeneous surface and energy of adsorption sites was inequality, and the Freundlich isotherm equation is expressed as [39]:

$$\ln q_e = \ln K_F + \frac{1}{n} \ln C_e \text{(linear)} \tag{7}$$

$$q_e = K_F C_e^{\frac{1}{n}} \text{(non - linear)} \tag{8}$$

where q_e (mg/g) and C_e (mg/L) are the uranium amount adsorbed on the sorbent at equilibrium and the equilibrium uranium(VI) concentration respectively, the q_m (mg/g) is the maximum adsorption amount of solute adsorbed per unit weight of MHC-PA for uranium(VI), K_L (L/mg) is the Langmuir equilibrium adsorption constant, which is related to the energy of sorption. K_F ((mg/g) (L/mg)1/n) and n are the Freundlich equilibrium adsorption constant which denote the extent of adsorption and the degree of nonlinearity between

solution concentration and adsorption respectively being determined from the intercept and slope of the linear plot of $\ln q_e$ against $\ln C_e$ in Fig. 12a [40]. All the results were listed in Table 3. The fitting results of temkin and D–R models were shown as Fig. s4 snd Table s2 in the supporting material.

Comparing of R^2 value of the four kinds of models, it can be seen from the Table 3 and Table s2 that the linear Langmuir model and the Temkin model with high correlation coefficients (R^2) were more suitable for describing the

adsorption process of uranium by MHC-PA microspheres. This result suggested that physisorption and the monolayer chem-adsorption happened on the homogeneous surface of MHC-PA microspheres simutaneously [41].

According to Table 4, the separation factor (RL) of U(VI) adsorbed by CMKGM/GG-Al microspheres at different temperatures and concentrations were all between 0 and 1. This indicated that the adsorption of U(VI) by CMKGM/GG-Al microspheres was favorable under the experimental conditions in this paper.
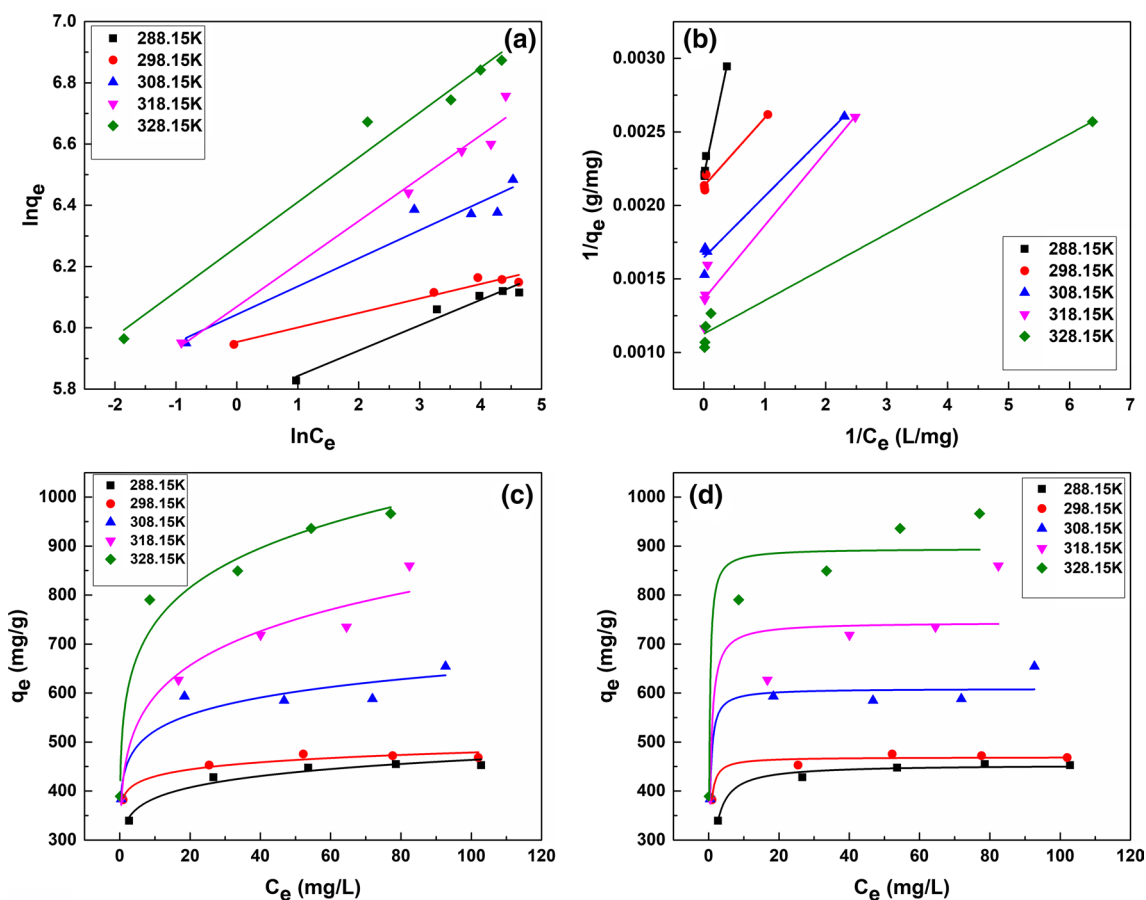
Fig. 12 **a**, **c** The linear and non-linear fitting of Freundlich model and **b**, **d** the linear and non-linear fitting of Langmuir model for uranium(VI) adsorption on MHC-PA

Table 3 The parameters for Langmuir and Freundlich models

Type	T (K)	Langmuir			Freundlich		
		q_m (mg/g)	K_L (L/mg)	R^2	K_F (mg/g)(L/mg)$^{1/n}$	n	R^2
Linear model	288.15	359.712	0.993	0.985	255.356	12.384	0.958
	298.15	423.729	3.537	0.963	355.317	23.425	0.952
	308.15	598.802	1.275	0.963	364.541	8.247	0.918
	318.15	694.444	1.833	0.914	401.148	7.126	0.971
	328.15	840.336	5.479	0.978	497.816	6.739	0.972

Table 4 The separation factor R_L ($R_L = 1/(1 + K_L * C_0)$) [42, 43]

Type	Temperature (K)	20 ppm	50 ppm	80 ppm	110 ppm	140 ppm
Linear model	288.15	0.048	0.020	0.012	0.009	0.007
	298.15	0.014	0.006	0.004	0.003	0.002
	308.15	0.038	0.015	0.010	0.007	0.006
	318.15	0.027	0.011	0.007	0.005	0.004
	328.15	0.009	0.004	0.002	0.002	0.001

Effect of temperature on adsorption

The effect of temperature ranging from 288.15 to 328.15 K on adsorption was studied at the initial uranium concentrations ranging from 20 to 140 mg/L and the results were displayed in Fig. 13.

It can be observed from Fig. 13a that the uranium amount adsorbed on the MHC-PA increased slightly along with the increase of temperature at low concentrations. This may be due to the limited amount of U(VI) in the low concentration solution and the existence of a large number of empty active centers on the surface of the adsorbent, so the effect of temperature on the adsorption is not obvious at low concentration. However, at high concentration, the adsorption amount increases rapidly with the increase of temperature, which may be because the increase of temperature accelerated the probability of collision between adsorbent molecules and uranium(VI), therefore, temperature played a major role at high concentrations.

In order to profoundly evaluate the principle of temperature influencing on adsorption amount, three basic thermodynamic parameters (ΔG^0, ΔH^0, ΔS^0) of adsorption were calculated using the following equations [43]:

$$K_0 = q_m \times K_L \tag{9}$$

$$\ln K_0 = \frac{-\Delta H^0}{R} \times \frac{1}{T} + \frac{\Delta S^0}{R} \tag{10}$$

$$\Delta G^0 = -RT \ln K_0 \tag{11}$$

where R (8.314 J/(mol K)) is the ideal gas constant, K_0 denotes the distribution coefficient equal to $q_m \times K_L$ of the Langmuir isotherm [44], ΔH^0 (kJ/mol), ΔS^0 (J/mol K), and ΔG^0 (kJ/mol) are enthalpy change, entropy change and Gibbs free energy change in a given process, respectively. Among them, enthalpy change (ΔH^0) and entropy change (ΔS^0) were calculated based on the slope and intercept of the straight line (Fig. 13b) using the following Eq. (9), Gibbs free energy change (ΔG^0) can be calculated according to Eq. (10) and (11).

A linear plot of $\ln K_0$ versus $1/T$ for uranium adsorption by MHC-PA was shown in Fig. 13b, the calculated parameters of ΔH^0, ΔS^0, and ΔG^0 were summarized in Table 5. Obviously, the positive values of ΔH^0 at all temperatures reflected that the adsorption of uranium(VI) onto MHC-PA microspheres process was endothermic, while positive ΔS^0 values indicated the increased randomness between the solid and
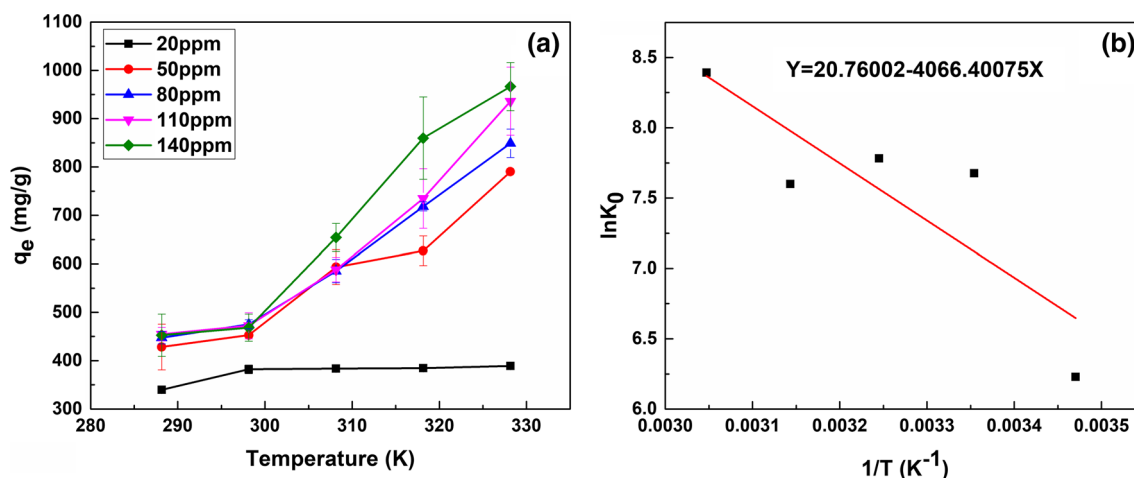
Fig. 13 a The effect of temperature on the adsorption of uranium(VI) onto the MHC-PA and **b** the plot of ln K_0 versus $1/T$ for the adsorption of uranium(VI) onto the MHC-PA (t: 24 h, pH: 4.5, V: 100 mL and m: 0.005 g)

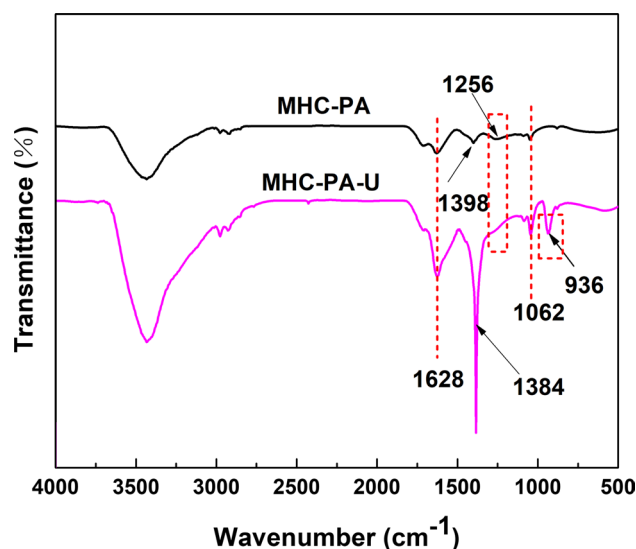**Table 5** Thermodynamic parameters for the uranium(VI) adsorption onto MHC-PA

Adsorbents	ΔH^0 (kJ/mol)	ΔS^0 (J/mol K)	ΔG^0 (kJ/mol)				
			288.15	298.15	308.15	318.15	328.15
MHC–COOH	23.70	121.08	−10.09	−13.20	−13.19	−13.41	−13.50
MHC-PA	33.81	172.60	−14.92	−19.03	−19.94	−20.10	−22.90
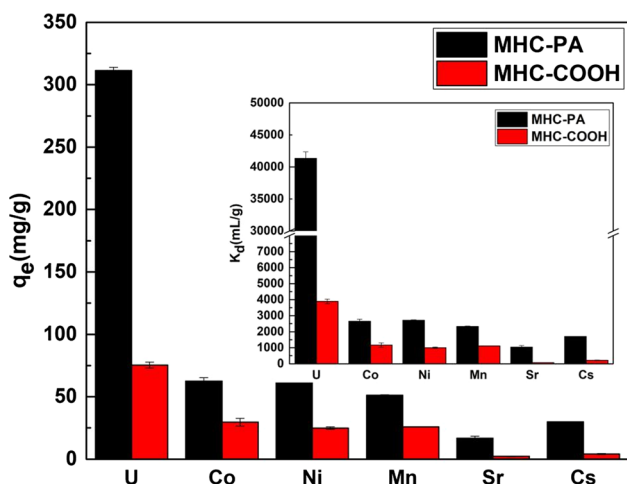
Fig. 14 The effect of coexisting ions on the adsorption of uranium(VI) by MHC-PA

Fig. 15 FTIR of before and after U(VI) adsorption of MHC-PA

aqueous solution interface during the adsorption process. In addition, the negative value of ΔG^0 demonstrated the feasibility and spontaneous for removal of uranium(VI) under all test conditions. It was found that the absolute value of ΔG^0 increased with increasing the temperature ranging from 288.15 to 328.15 K, suggesting that the higher temperature was more efficient to adsorption process. Furthermore, the ΔG^0 of MHC-PA during the adsorption process were greater than that of MHC-COOH at the temperatures of 288.15 K to 328.15 K respectively. It suggested that MHC-PA were more favorable for to capture uranium.

Effect of coexisting ions on adsorption of uranium(VI)

As the waste water of nuclear industry contains not only uranium ions but also other metal cations, which may have some influence on the adsorption uranium of materials, this paper explores the influence of five kind of Co^{2+}、Ni^{2+}、Mn^{2+}、Sr^{2+} and Cs^+ coexisting ions on the adsorption uranium of MHC-PA [24], and the results are shown in Fig. 14. It can be seen from the figure that the adsorption capacity of MHC-PA for uranium(VI) is significantly higher than that of other five cations, while the adsorption capacity of MHC-PA for other ions is very low, especially for Sr^{2+} and Cs^+. Compared with MHC-COOH without grafting phytic acid, the adsorption capacity of MHC-PA to uranium is nearly 4 times that of MHC-COOH,

which shows that the adsorption capacity of MHC-COOH is greatly improved through the modification by phytic acid. It can also be found that the K_d (41,328.76 mL/g) value of MHC-PA is significantly higher than that of MHC-COOH (3895.14 mL/g), which indicates that the phytic acid modified MHC-COOH can greatly improve the selective adsorption of uranium. In general, the modification of MHC-COOH by phytic acid increased the adsorption sites of MHC-PA for uranium, increased the adsorption capacity and selectivity of uranium.

Mechanism analysis

FTIR

The functional groups of MHC-PA before and after adsorption (MHC-PA-U) were analyzed by FTIR, as shown in Fig. 15. The absorption peak at 1628 cm^{-1} belongs to C=C stretching vibration peak, the absorption peak at 1398 cm^{-1} belongs to C–H bending vibration peak, the absorption peak at 1062 cm^{-1} belongs to P–O–C group vibration peak, and the absorption peak at 1256 cm^{-1} belongs to P=O vibration peak. After adsorption of U(VI), a new characteristic peak appears at 936 cm^{-1} in the FTIR curve of MHC-PA-U [45], Besides, after the adsorption of U(VI), the absorption peak at 1398 cm^{-1} shifts to 1384 cm^{-1}, and the intensity of the

peak at 1256 cm^{-1} almost disappeared, suggesting that there was a interaction between oxygen atom and U(VI).

EDX

The SEM and EDX of MHC-PA before and after the adsorption of U(VI) are shown in Fig. 16. It can be seen from Fig. 16a, b that the surface of carbon microspheres is barely changed before and after the adsorption of U(VI), indicating that the surface structure of MHC-PA microspheres is relatively stable. Figure 16c shows the EDX comparison before and after adsorption of U(VI). The appearance of U(VI) element in the EDX diagram after adsorption indicates that U(VI) is successfully adsorbed by MHC-PA. It can be also found that the U(VI) element is evenly distributed on the surface of carbon microspheres, which was revealed through the surface scanning distribution of the U(VI) elements adsorbed on the surface MHC-PA, as shown in Fig. 16d–g.

XPS

From those above FT-IR and EDX results, we can concluded that U(VI) have been successfully adsorbed on the MHC-PA. To further understand the interaction mechanism of U(VI) and MHC-PA, the XPS spectra before and after adsorption of U(VI) and the high resolution scans of U 4f, P 2p and O 1 s were recorded and showed in Fig. 17.

As shown in Fig. 17a, the obvious double peaks of U 4f appeared in XPS spectrum of the MHC-PA-U, indicating the successful adsorption of U(VI) by MHC-PA. The high resolution scans of U 4f including U $4f_{7/2}$ and U $4f_{5/2}$ appeared at ~ 382 and ~ 393 eV, seen in Fig. 17d, respectivly,

indicated the successful formation of bidentate complex during adsorption [46].

Figure 17e concluded the detail spectra of O 1 s at 531.73 eV, 532.64 eV, 533.17 eV, 533.77 eV before adsorption of U(VI). After adsorption of U(VI), those peakes shifted to 533.51 eV, 531.40 eV, 532.78 eV, 533.55 eV respectively seen in Fig. 17f. Moreover, the relative intensity of these peaks decreased. Compared with MHC-PA, the peaks of P 2p (Fig. 17b) at 133.09 eV, 139.9 eV shifted to 132.07 eV, 134.70 eV of MHC-PA-U (Fig. 17c). Thus it can be inferred from the above results that the chelatation of U(VI) with P=O and P-OH is formed by the electron sharing of uranium ion and oxygen atom.

The possible formation mechanism and the U(VI) adsorption mechanism of MHC-PA were deduced from the above adsorption model and characterization. The corresponding schematic diagram is shown in Fig. 18. Specifically, the surface of calcined microwave-assisted hydrothermal carbon (MHC-COOH) is rich in carboxyl and hydroxyl functional groups. Phytic acid is a functional monomer containing six phosphate groups. In the process of hydrothermal modification, the hydrogen bonding was formed by –C=O on the surface of MHC-COOH and P–OH on the surface of phytic acid in the aqueous solution leadin to the successfully modification of microwave assisted hydrothermal carbon (MHC-COOH) with the phytic acid.

Based on the results before including the adsorption fitting model and various characterization, the adsorption of uranium on MHC-PA carbon microspheres is mainly chemical adsorption. The main chemical process were the coordination action of uranyl ions with oxygen containing groups including P=O and P–OH on MHC-PA which results in the
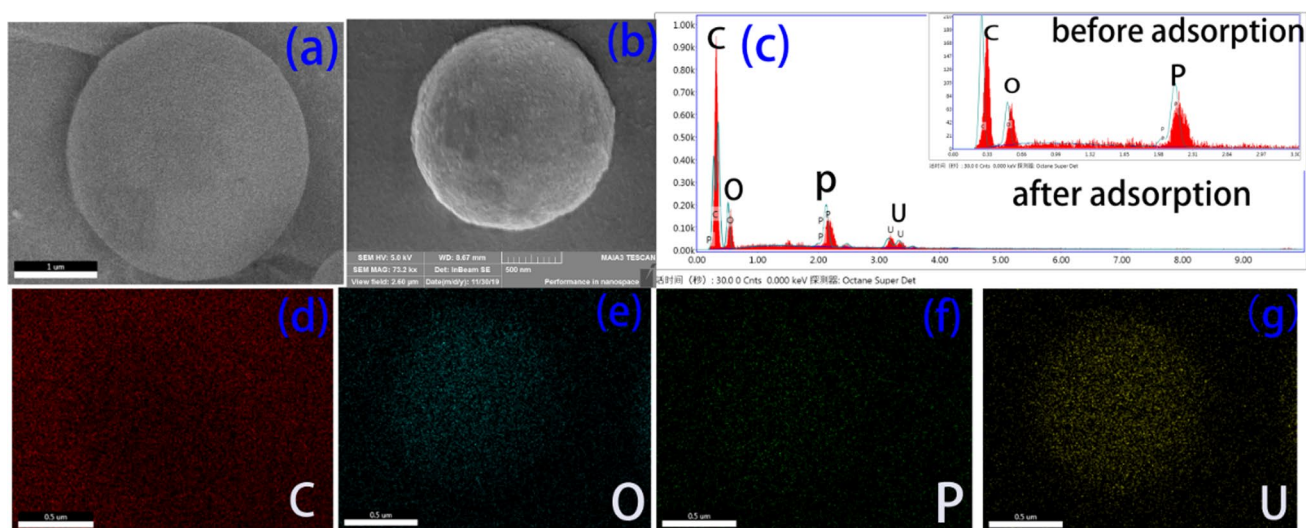
Fig. 16 **a** and **b** SEM before and after adsorption of U(VI); **c** EDX before and after adsorption of U(VI) by MHC-PA; **d–g** surface scanning distribution of surface elements after adsorption of U(VI) by MHC-PA
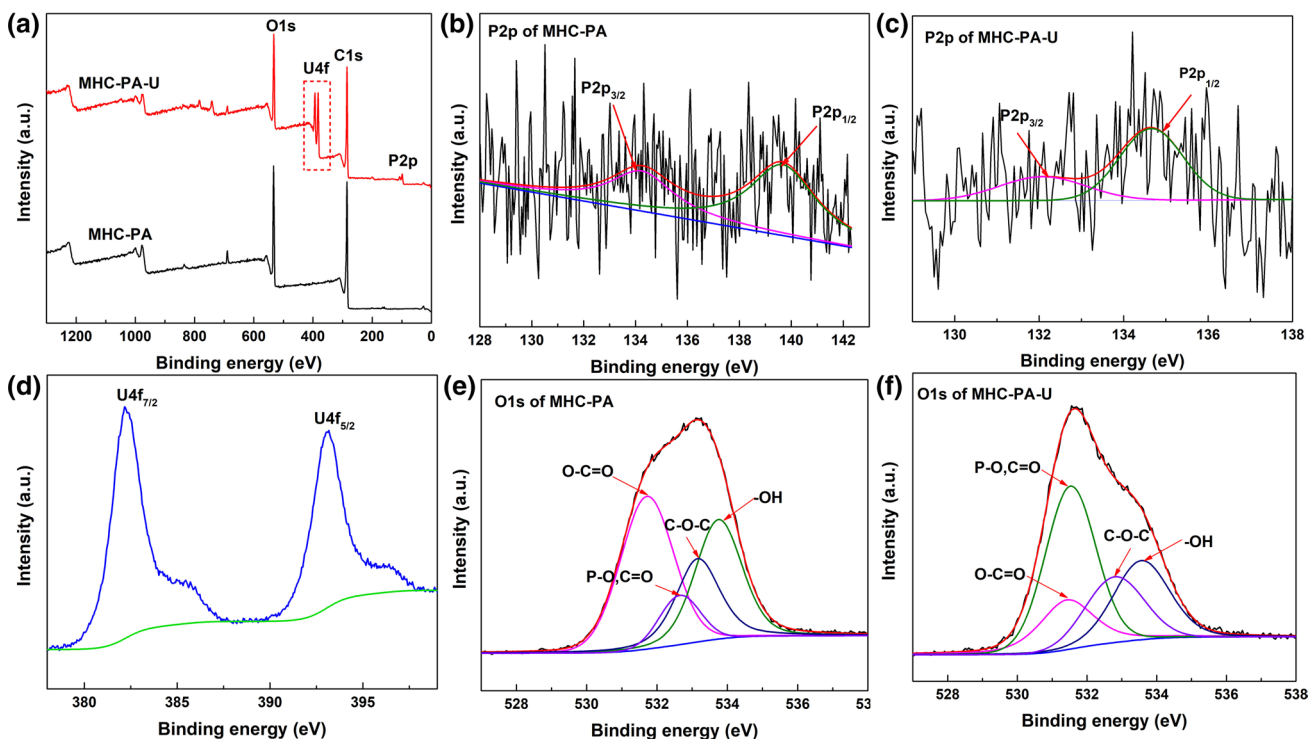
Fig. 17 XPS spectra of **a**, **d** MHC-PA and MHC-PA-U; **b** P 2p and **e** O 1 s for MHC-PA; **c** P 2p and **f** O 1 s for MHC-PA-U
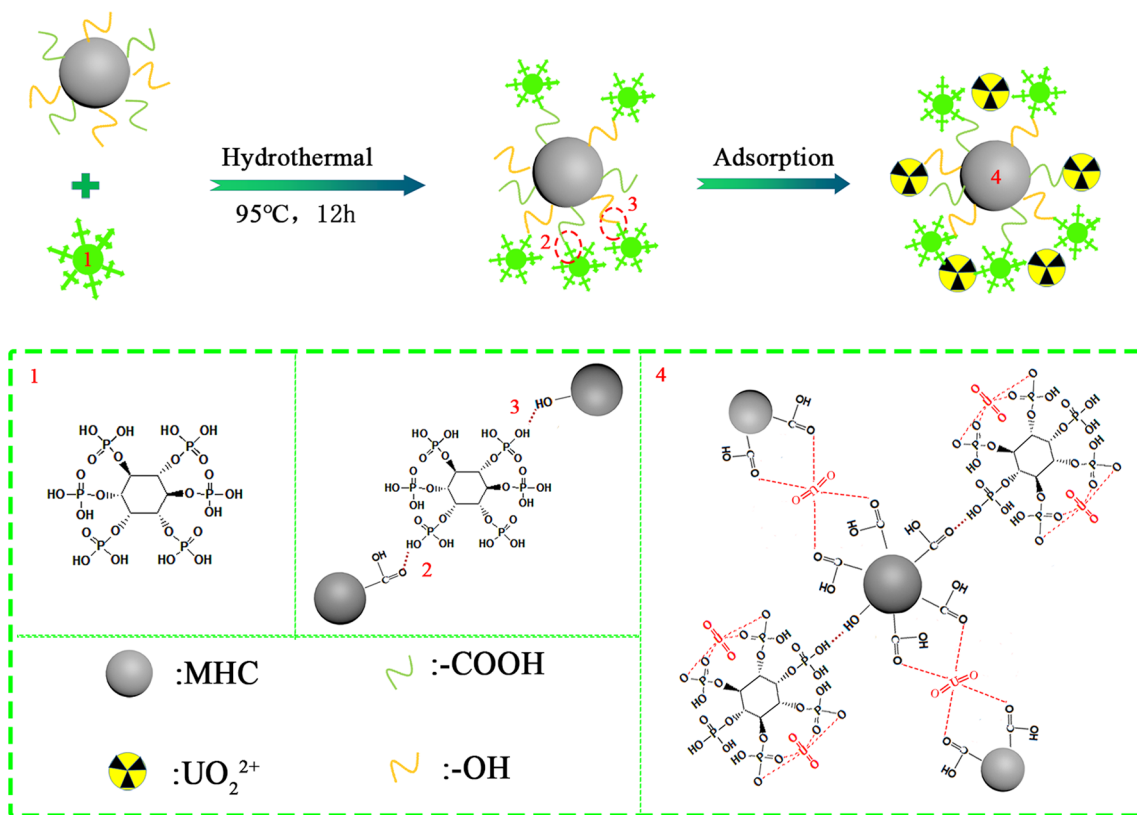

Fig. 18 Schematic illustration of the formation mechanism of MHC-PA and the adsorption mechanism of MHC-PA for U(VI)

adsorption of U(VI) on the surface of adsorbent MHC-PA. Due to the strong chelating ability of phytic acid to uranium, the MHC-PA has excellent adsorption performance for U(VI) than MHC-COOH.

Conclusion

In the present work, MHC-PA and MHC-STPP were successfuly synthesized by the environmental friendly hydrothermal method at 95 °C low temperature, using phytic acid and sodium tripolyphosphate as modifiers, respectivly. The morphology, structure, surface composition of MHC-PA and MHC-STPP were characterized. The results showed that the hydrogen bonding between phytic acid and carbon microsphere made the PA modified hydrothermal carbon stick obviously and the sodium tripolyphosphate functionalization reduces the particle size of the hydrothermal carbon to nanometer level, but the surface morphology has no significant effect. Phytic acid and sodium tripolyphosphate only react with the surface groups of the hydrothermal carbon microspheres.

Adsorption performance of MHC-PA for U(VI) was investigated by batch experiments, including the influence of pH, absorbent dose, initial uranium concentration, contact time and temperature on adsorption. The adsorption results showed that the maximum adsorption capacity increased from 53 of MHC-COOH to 382 mg/g of MHC-PA by functional modification of PA. The adsorption process of uranium is more in line with Langmuir isothermal model and Pseudo-second-order kinetic model, which shows that the adsorption process is dominated by monolayer chemical adsorption process and physical adsorption. The thermodynamic analysis showed that the adsorption process of U(VI) by MHC-PA was endothermic and spontaneous. The main adsorption mechanism of MHC-PA for U(VI) mainly the chelation of U(VI) with P=O, P–OH functional group and the electrostatic action.

In all, MHC-PA would be an promising adsorbent with excellent adsorption performance, eco friendliness and cost effectiveness for removal U(VI) from aqueous solution.

References

1. Anirudhan TS, Bringle CD, Rijith S (2010) Removal of uranium(VI) from aqueous solutionsand nuclear industry effluents using humic acid-immobilized zirconium-pillared clay. J Environ Radioact 101:267–276

2. Zhang CL, Li X, Chen ZS, Wen T, Huang SY, Hayat T, Alsaedi A, Wang XK (2018) Synthesis of ordered mesoporous carbonaceous materials and their highly efficient capture of uranium from solutions. Sci China Chem 61:281–293

3. Aly Z, Luca V (2013) Uranium extraction from aqueous solution using dried and pyrolyzed tea and coffee wastes. J Radioanal Nucl Chem 295:889–900

4. Torkabad MG, Keshtkar AR, Safdari SJ (2017) Comparison of polyethersulfone and polyamide nanofiltration membranes for uranium removal from aqueous solution. Prog Nucl Energy 94:93–100

5. Duan SX, Liu X, Wang YN, Shao DD, Alharbi NS, Alsaedi A, Li JX (2016) Highly efficient entrapment of U(VI) by using porousmagnetic $Ni_{0.6}Fe_{2.4}O_4$ micro-particles asthe adsorbent. J Hazard Mater 65:367–377

6. Mustafa T, Tawfik AS, Ahmet S, Naeemullah (2020) Interfacial polymerization of trimesoyl chloride with melamine and palygorskite for efficient uranium ions ultra-removal. Chem Eng Res Des 159:353–361

7. Esra B, Ahmet S, Mustafa T (2018) Effective uranium biosorption by macrofungus (Russula sanguinea) from aqueous solution: equilibrium, thermodynamic and kinetic studies. J Radioanal Nucl Chem 317:1387–1397

8. Tawfik AS, Naeemullah Mustafa T, Ahmet S (2017) Polyethylenimine modified activated carbon as novel magnetic adsorbent for the removal of uranium from aqueous solution. Chem Eng Res Des 117:218–227

9. Niu YH, Lu ZY, Li J, Jiang J, Lu J, Wu KP (2019) Low-cost synthesis of cellular materials with preformed foam for uranium(VI) adsorption. Mater Lett 247:36–39

10. Lai ZJ, Zhang ZB, Cao XH, Dai Y, Hua R, Le ZG, Luo MB, Liu YH (2016) Synthesis of novel functional hydrothermal carbon spheres for removal of uranium from aqueous solution. J Radioanal Nucl Chem 310:1335–1344

11. Zheng ZY, Wang YQ, Zhao WW, Xiong GX, Cao XH, Dai Y, Le ZG, Yu SL, Zhang ZB, Liu YH (2017) Adsorptive removal of uranyl ions in aqueous solutionusing hydrothermal carbon spheres functionalizedwith 4-aminoacetophenone oxime group. J Radioanal Nucl Chem 312:187–198

12. Zhang ZB, Liu YH, Cao XH, Liang P (2013) Sorption study of uranium on carbon spheres hydrothermal synthesized with glucose from aqueous solution. J Radioanal Nucl Chem 295:1775–1782

13. Adolfsson KH, Lin CF, Hakkarainen M (2018) Microwave assisted hydrothermal carbonization and solid state postmodification of carbonized polypropylene. ACS Sustain Chem Eng 6:11105–11114

14. Alexandre L, Hibiki U, Ryo T, Polina M, Naritaka K, Ryuzo K, Seiichiro N (2017) Monitoring and extraction of uranium in polluted acid mine drainage by super-paramagnetic nanoparticles coated with carbon nanodots. J Radioanal Nucl Chem 314:1149–1159

15. Xu DD, Xu TY, Guo XJ, Liu Q, Liu JY, Lv WZ, Jing XY, Zhang HS, Wang J (2017) Effect of the synthesis method on the performance of Fe_3O_4–inositol hexaphosphate as a drug delivery vehicle for combination therapeutics with doxorubicin. New J Chem 41:5305–5312

16. Lei H, Pan N, Wang XQ, Zou H (2018) Facile synthesis of phytic acid impregnated polyaniline for enhanced U(VI) adsorption. J Chem Eng Data 63:3989–3997

17. Wang J, Wen X, Yang F, Cao ZF, Wang S, Zhong H (2018) Preparation of a novel two-dimensional carbon material and enhancing Cu(II) ions removal by phytic acid. Environ Earth Sci 77:472

18. Liu SJ, Ma JG, Zhang WQ, Luo F, Luo MB, Li FQ, Wu LP (2015) Three-dimensional graphene oxide/phytic acid composite for uranium(VI) sorption. J Radioanal Nucl Chem 306:507–514

19. Gurses MS, Erkey C, Kizilel S, Uzun A (2018) Characterization of sodiumtripolyphosphate and sodium citrate dehydrate residues on surfaces. Talanta 176:8–16

20. Chu HH, Lin XY, Li MS, Liang LL, Zhou J, Shang R, Luo XG (2019) Rapid synthesis of carbon materials by microwave-assisted hydrothermal method at low temperature and its adsorption properties for uranium(VI). J Radioanal Nucl Chem 321:629–646

21. Zhao WH, Lin XY, Cai HM, Mu T, Luo XG (2017) Preparation of mesoporous carbon from sodium lignosulfonate by hydrothermal and template method and its adsorption of uranium(VI). Ind Eng Chem Res 56:12745–12754

22. Chen Z, Ma LJ, Li SQ, Geng JX, Song Q, Liu J, Wang CL, Wang H, Li J, Qin Z, Li SJ (2011) Simple approach to carboxyl-rich materials through low-temperature heat treatment of hydrothermal carbon in air. Appl Surf Sci 257:8686–8691

23. Fanning PE, Vannice MA (1993) A DRIFTS study of the formation of surface groups on carbon by oxidation. Carbon 31:721–730

24. Pan N, Jin YD, Wang XQ, Hu XP, Chi FT, Zou H, Xia CQ (2019) A self-assembled supramolecular material containing phosphoric acid for ultrafast and efficient capture of uranium from acidic solutions. ACS Sustain Chem Eng 7:950–960

25. Li HY, Liu L, Zhang ZW, Wang SS, Yu Y, Liu L, Wu Y (2017) Phytic acid-assisted electrochemically synthesize three-dimensional O, P-functionalized graphene monolith with high capacitive performance. Nanoscale 9:12601–12608

26. Ehsanjoo M, Mohammadi S, Chaibakhsh N (2019) Long-term corrosion resistance of zinc-rich paint using functionalised multilayer graphene-tripolyphosphate: in situ creation of zinc phosphate as corrosion inhibitor. Corros Eng Sci Technol 54:698–714

27. Yu J, Luo XG, Liu B, Zhou J, Feng J, Zhu WK, Wang SL, Zhang YD, Lin XY, Chen P (2018) Bayberry Tannin immobilized bovine serum albumin nanospheres: characterization, irradiation stability and selective removal of uranyl ion from radioactive wastewater. J Mater Chem A 6:15359–15370

28. Cai YW, Wu CF, Liu ZY, Zhang LJ, Chen LH, Wang JQ, Wang XK, Yang ST, Wang S (2017) Fabrication of phosphorylated graphene oxide-chitosan composite for highly effective and selective capture of U(VI). Environ-Sci Nano 4:1876–1886

29. Liao Y, Wang M, Chen DJ (2019) Electrosorption of uranium(VI) by highly porous phosphate-functionalized graphene hydrogel. Appl Surf Sci 484:83–96

30. Ding CC, Cheng WC, Nie XQ, Yi FC (2017) Synergistic mechanism of U(VI) sequestration by magnetite-graphene oxide composites: evidence from spectroscopic and theoretical calculation. Chem Eng J 324:113–121

31. Zhang ZB, Dong ZM, Dai Y, Xiao SJ, Cao XH, Liu YH, Guo WH, Luo MB, Le ZG (2016) Amidoxime-functionalized hydrothermal carbon material for uranium removal from aqueous solution. RSC Adv 6:102462–102471

32. Monier M, Elsayed NH (2014) Selective extraction of uranyl ions using ion-imprinted chelating microspheres. J Colloid Interface Sci 423:113–122

33. Wu LP, Lin XY, Du XC, Luo XG (2016) Biosorption of uranium(VI) from aqueous solution using microsphere adsorbents of carboxymethyl cellulose loaded with aluminum(III). J Radioanal Nucl Chem 310:611–622

34. Zhang YH, Lin XY, Zhou QS, Luo XG (2016) Fluoride adsorption from aqueous solution by magnetic core-shell Fe3O4@alginate-La particles fabricated via electro-coextrusion. Appl Surf Sci 389:34–45

35. Sivakami MS, Gomathi T, Venkatesan J, Jeong HS, Kim SK, Sudha PN (2013) Preparation and characterization of nano chitosan for treatment wastewaters. Int J Biol Macromol 57:204–212

36. Liu YH, Wang YQ, Zhang ZB, Cao XH, Nie WB, Li Q, Hua R (2013) Removal of uranium from aqueous solution by a low cost and high-efficient adsorbent. Appl Surf Sci 273:68–74

37. Anirudhan TS, Lekshmi GS, Shainy F (2018) Synthesis and characterization of amidoxime modified chitosan/bentonite composite for the adsorptive removal and recovery of uranium from seawater. J Colloid Interface Sci 534:248–261

38. Nilchi A, Dehaghan TS, Garmarodi SR (2013) Kinetics, isotherm and thermodynamics for uranium and thorium ions adsorption from aqueous solutions by crystalline tin oxidenanoparticles. Desalination 321:67–71

39. Sureshkumar MK, Das D, Mallia MB, Gupta PC (2010) Adsorption of uranium from aqueous solution using chitosan-tripolyphosphate(CTPP)beads. J Hazard Mater 184:65–72

40. Chen JF, Zhang WY, Li X (2016) Adsorption of Cu(II) ion from aqueous solutions on hydrogel prepared from Konjac glucomannan. Polym Bull 73:1965–1984

41. Anirudhan TS, Nima J, Divya PL (2015) Adsorption and separation behavior of uranium(VI) by 4-vinylpyridine-grafted-vinyltriethoxysilane-cellulose ion imprinted polymer. J Environ Chem Eng 3:1267–1276

42. Bayramoglu G, Arica MY (2016) MCM-41 silica particles grafted with polyacrylonitrile: modification into amidoxime and carboxyl groups for enhanced uranium removal from aqueous medium. Microporous Mesoporous Mater 226:117–124

43. Li J, Zhang SW, Chen CL, Zhao GX, Yang X, Li JX, Wang XK (2012) Removal of Cu(II) and fulvic acid by graphene oxide nanosheets decorated with Fe₃O₄ nanoparticles. ACS Appl Mater Interfaces 4:4991–5000

44. Zhou QS, Lin XY, Qian J, Wang J, Luo XG (2015) Porous zirconium alginate beads adsorbent forfluoride adsorption from aqueous solutions. RSC Adv 5:2100–2112

45. Geng JX, Ma LJ, Wang H, Liu J, Bai CY, Song Q, Li J, Hou M, Li SJ (2012) Amidoxime-grafted hydrothermal carbon microspheres for highly selective separation of uranium. J Nanosci Nanotechnol 12:7354–7363

46. Wang Y, Gu ZX, Yang JJ, Liao JL, Yang YY, Liu N, Tang J (2014) Amidoxime-grafted multiwalled carbon nanotubes by plasma techniques for efficient removal of uranium(VI). Appl Surf Sci 320:10–20